Performance simulation of perovskite solar cell with $Ti_3C_2T_X$ MXene as the HTL

Margdaline Musanga Ligavo[1], Sebastian Waita[1], Francis Wanjala Nyongesa[1] Mmantsae Diale[2]

[1]Department of Physics, University of Nairobi, P. O. Box 30197 – 00100, Nairobi, Kenya

[2]Department of Physics, University of Pretoria, Private Bag X20, Hatfield, 0028, South Africa

Abstract

Lately, the use of 2D transitional metal carbides (MXene) in perovskite solar cells (PSC) due to their favorable properties like high carrier mobility, high electrical conductivity and tunable work function, has gained significant attention. The use of $Ti_3C_2T_x$ as HTL in perovskite experimentally has been reported. In this work, a simulation of perovskite solar cell incorporating $Ti_3C_2T_x$ MXene as hole transport layer (HTL) using SCAPS-1D software has been presented. A numerical investigation of the effect of ETL, HTL, and absorber doping concentration; absorber defect density; absorber/ETL and absorber/HTL interface defect density, and HTL thickness on the device photovoltaic performance has been explored. After optimization, the metric parameters obtained were; V_{OC} = 0.9287 V, J_{SC} = 21.43 mA/cm^2, FF = 70.90 % and PCE = 14.11%. Comparing the simulated and experimental results reported shows that optimizing the MXene thickness, doping concentrations and defect densities improves the device's photovoltaic performance.

Keywords: MXene, SCAPS-1D, perovskite, photovoltaic performance

1. INTRODUCTION

Perovskite solar cells (PSCs) have gained extensive research attention due to their excellent optoelectronic properties like tunable band gap, high optical absorbency factor, low exciton binding energy, high carrier diffusion length and low manufacturing cost. Since PSCs were first reported in 2009, their PCE has tremendously risen from 3.8 % to an impressive value of 26.1 % for over a decade indicating their great potential as substitutes for the dominant silicon-based solar cells (Liu et al., 2023). Despite the remarkable PCE reported, the practical application of the PSCs is still inhibited by factors such as oxygen, light, and thermal stability, and large scale reproducibility and low PCE obtained by large scale modules (Diouf et al., 2023; Yang et al., 2024). Several approaches have been employed to enhance the stability and hence efficiency of PSCs including incorporating stabilizing agents, fabricating devices in an inert environment and designing PSCs basing on innovative device architectures (Baraneedharan et al., 2024). Lately, the application of 2D transitional metal carbides (MXenes) in PSCs has gained much attention. MXenes are prepared by selectively etching the A layer from the MAX ($M_{n+1}AX_n$) precursors, where M is a transitional metal such as Mo, Zr, Ti, Cr, A stands for an A-group element like Al, Ge, Si, Ga while X takes oxygen or carbon or a mixture and n=1 to 3 (Babar et al., 2023). The general formula for MXenes is $M_{n+1}X_nT_x$ where n varies between 1 & 3 and T represents -O, -F and/or -OH functional groups which form due to the reaction with acids during the etching process. MXenes exhibits three lattice structures namely M_2X, M_3X_2, and M_4X_3 comprising 3, 5 or 7 atomic layers respectively (Salim et al., 2019). MXenes exhibit distinctive properties like tunable band gap and work function, high optical transparency high charge mobility that make them suitable for production of more efficient large-scale PSCs. In addition, these 2D materials can inhibit moisture induced decomposition of the PSC boosting their stability. MXenes can be utilized as HTLS, ETLS, additives, interlayers and electrodes in PSCs to improve efficient charge extraction and film quality enhancing their photovoltaic performance (Qamar et al., 2022; Yang et al., 2023).

TiC_3T_x Mxene was the first to be discovered and is the most widely studied. It possess excellent properties like flexibility, hydrophilicity, high electrical conductivity and the ease of preparation from aqueous solutions (Du et al., 2022a; Yang et al., 2023). The use of TiC_3T_x Mxene as an additive in the PSC absorber material was first reported by Guo et al. (2018). They found that due to its high electrical conductivity and charge mobility,

© 2026. The Authors. Published by International Solar Energy Society
Selection and/or peer review under responsibility of Scientific Committee
10.18086/swc.2025.03.55 Available at http://proceedings.ises.org

the Mxene, enhanced charge transfer improving the device's PCE. In addition, they reported that the termination groups in the Mxene slowed down the crystallization process of the perovskite hence increasing the film's crystal sizes. With 0.03 wt% TiC_3Tx additive, a PCE of 17.41 %, V_{OC}, FF, J_{SC} of 1.03 V, 0.76 and 22.26 mA/cm^2 respectively were obtained outperforming the performance of the pristine device which produced a PCE of 15.54 %, J_{SC} = 20.67 mA/cm^2, V_{OC} = 1.00 V and FF = 0.75. TiC_3T_x Mxene demonstrated its potential to be used an ETL in PSC for instance, Wang et al. (2021) fabricated PSC with TiC_3T_x ETL through the room temperature solution process followed by oxygen plasma treatment. They observed that modifying the surface of the Mxene via oxygen plasma treatment broke partly the Ti-C bonds randomly liberating the Ti-O bonds on the Mxene surface resulting in tunable work function, a decrease in trap states an enhanced transportation of electrons near the interface enhancing the device PCE. Pb-O interactions amid the perovskite and Mxene lead to improved device stability. The champion device was obtained for plasma treatment of 3 min producing a V_{OC}, J_{SC}, FF and PCE of 1.03 V, 24.17 mA/cm^2, 80.0 % and 19.92 % respectively. The application of TiC_3T_x Mxene incorporated with varying amounts of silane coupling agent (SCA) vinyltris i.e 2-methoxyethoxysilane as HTL in PSC through spray coating technique was reported by Du et al. (2022).They observed that introducing SCA in TiC3Tx films by spray coating enabled formation good quality films that enhanced device PCE from 11.12 % to 13.65 % due to enhanced hole extraction, hole transfer and low mobility resistance at the HTL/perovskite interface.

The PCE obtained for PSC with TiC_3T_x Mxene as HTL is still relatively low, hence it is imperative to explore further on ways of optimizing parameters that would maximize the PCE obtained using this material. Hence in this work, we present a simulation of planar inverted PSC with TiC_3T_x Mxene as HTL (ITO/Ti_3C_2Tx/$MAPbI_3$/PCBM/Ag) and provide an optimization procedure for the device's ETL, HTL, absorber doping concentrations, Mxene thickness, absorber and interface defect densities using the solar cell capacitance simulator (SCAPS-1D) software.

2. NUMERICAL MODELLING AND SIMULATION

Device structure and simulation approach

Figure 1(a) &(b) depicts the simulated inverted p-i-n planar structure of perovskite solar cell and the corresponding energy band diagram, respectively. The planar structure consists of a transparent conductive oxide (TCO) layer, a hole transport layer (HTL), an absorber layer, an electron transport layer (ETL), and a metallic back contact. Indium-doped tin oxide (ITO) as the TCO, and silver Ag with a work function of 4.74 eV (He et al., 2020) was used as the back metal contact. $MASnI_3$ is the absorber layer sandwiched between the HTL and the ETL. $Ti_3C_2T_X$ MXene was used as HTL while [6,6]-phenyl-C_{60}-butyric acid methyl ester (PCBM) is used as the ETL.

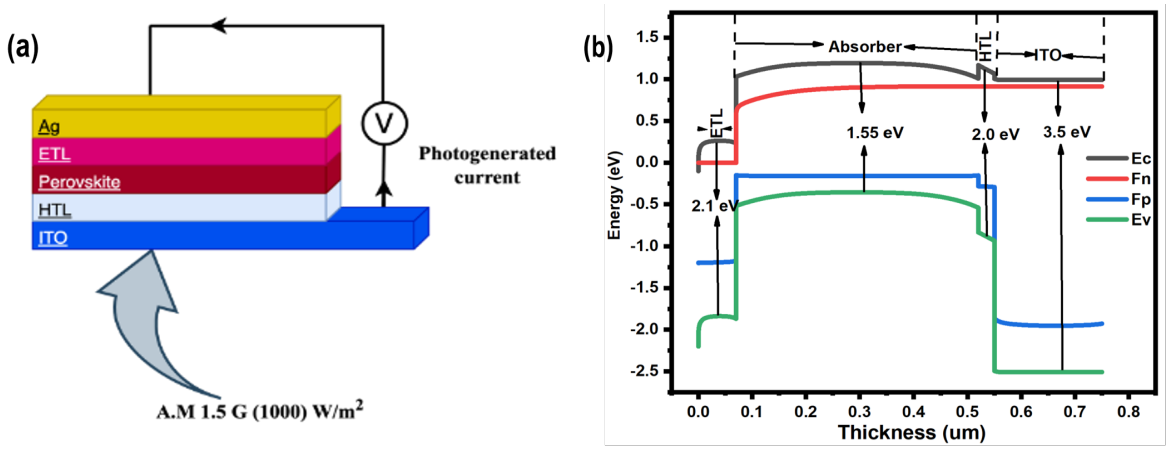

Figure 1(a) Structure (b) Energy band diagram for the simulated device

The solar cell capacitance simulator (SCAPS-1D) software, version 3.3.11, developed at the Department of Electronics and Information Systems (ELIS) at the University of Ghent in Belgium (Burgelman et al., 2000), was used to simulate the PSC and investigate the influence of doping concentration, defect density, and MXene thickness on the electrical properties of the perovskite. The software computes the solar cell's outputs by

solving the Poisson equation and the electron and hole continuity equations shown in equation (1) and (2) (Nahid et al., 2024; Uddin et al., 2024):

$$\frac{d^2\varphi(x)}{dx^2} = \frac{e}{\varepsilon_o \varepsilon_r}(P(x) - n(x) + N_D - N_A + \rho_P - \rho_n) \quad \text{(eq. 1)}$$

where $\varphi(x)$ is the electrostatic potential, ie the potential energy that a test charge would have due to electric fields in the system, $P(x)$ &$n(x)$ represents the hole and electron concentration, respectively, N_D& N_A refer to donor and acceptor's charge impurities respectively, ρ_P & ρ_n are the holes' and electrons' density, e is the electric charge while ε_o & ε_r refer to the vacuum permittivity and relative permittivity respectively. The continuity equations for holes and electrons are presented in equation (2) and (3) , respectively (Karmaker et al., 2024)

$$\frac{dp_n}{d_t} = G_p - \frac{p_n - p_{no}}{\tau_p} - p_n\mu_p\frac{dE}{dx} - \mu_p E\frac{d_{pn}}{dx} + D_p\frac{d^2{}_{pn}}{dx^2} \quad \text{(eq. 2)}$$

$$\frac{dn_p}{d_t} = G_n - \frac{n_{p-}n_{po}}{\tau_n} - n_p\mu_n\frac{dE}{dx} - \mu_n E\frac{d_{np}}{dx} + D_n\frac{d^2 n_n}{dx^2} \quad \text{(eq. 3)}$$

where G_p and G_n stand for the hole and electron generation rates, respectively, D_p & D_n refer to the hole and electron diffusion coefficients, respectively, and μ_p & μ_n are the hole and electron mobilities respectively.

The carrier transport of electrons and holes is described by equation (4) and (5), respectively (Karmaker et al., 2024):

$$J_n(x) = qn\mu_n E + qD_n\frac{d_n}{dx} = n\mu_n\frac{dE_{Fn}}{dx} \quad \text{(eq. 4)}$$

$$J_p(x) = qp\mu_p E + qD_p\frac{d_p}{dx} = p\mu_p\frac{dE_{Fp}}{dx} \quad \text{(eq. 5)}$$

In the equations (4) and (5) E_F represents the quasi-Fermi levels while p and n, holes and electrons respectively.

Table1 shows the simulation parameters selected from published experimental work and other simulations. The simulation was carried out under illumination with A.M. 1.5 G and 1000W/m^2 spectrum, scanning voltage 0.5 V and 1 x 10^6 Hz frequency.

Table 1 Device simulation parameters

Parameters	**ITO (Bouderbala and Hamdi, 2023; Dar and Sengar, 2024; Yan et al., 2023)**	**MXene (Bhattarai et al., 2023; Hossain et al., 2023; Teli et al., 2025)**	**$MAPbI_3$ (Danladi et al., 2023; Hoy et al., 2025; Husainat et al., 2019)**	**PCBM (Jayan K and Sebastian, 2021; Sharma et al., 2024; Wang et al., 2015)**
Thickness (μm)	0.200	varied	0.450	0.070
Bandgap (eV)	3.5	2.0	1.55	2.1
Electron affinity (eV)	3.9	3.84	4.0	4.8
Dielectric permittivity	9.0	10.0	10.0	10.0
CB density of states (cm^{-3})	1.8×10^{19}	2.2×10^{18}	2.2×10^{18}	3.0×10^{21}
VB density of states (cm^{-3})	2.2×10^{19}	1.8×10^{18}	1.8×10^{19}	3.0×10^{21}
Electron thermal velocity (cm/s)	1.0×10^{7}	1.0×10^{7}	1.0×10^{7}	1.0×10^{7}
Hole thermal velocity (cm/s)	1.0×10^{7}	1.0×10^{7}	1.0×10^{7}	1.0×10^{7}
Electron mobility (cm^2/Vs)	2.0×10^{1}	1.0×10^{4}	1.0×10^{0}	1.0×10^{2}
Hole mobility (cm^2/Vs)	1.0×10^{1}	1.0×10^{4}	1.0×10^{0}	2.5×10^{0}
Donor density, N_D (cm^{-3})	9.0×10^{17}	0	0	1.0×10^{17}
Acceptor density, N_A (cm^{-3})	0	1.0×10^{15}	1.0×10^{16}	0
Defect density N_t (cm^{-3})	1.0×10^{14}	1.0×10^{14}	1.0×10^{14}	1.0×10^{14}

Table 2 depicts the input parameters for back and front contacts.

Parameters	Back contact	Front contact
Metal work function (eV)	4.74	Flat contact
Surface recombination velocity of electrons (cm^{-2}), σ_e	1×10^5	1×10^7
Surface recombination velocity of holes (cm^{-2}), σ_h	1×10^7	1×10^5

Table 3 indicates the interface properties set for this simulation.

Table 2 indicates the interface properties set for this simulation

Defect type	ITO/HTL interface	Absorber/ ETL interface	Absorber/ HTL interface
Capture cross section electrons (cm^2)	Neutral	Donor	Neutral
Capture cross section holes (cm^2)	1.00E-15	1.00E-15	1.00E-15
Energetic distribution	1.00E-15	1.00E-15	1.00E-15
Reference for defect energy level E_t	Single	Single	Single
Energy with respect to EV (eV)	0.500	0.500	0.500
Characteristic energy (eV)	0.1	0.1	0.1
Total density (integrated over all energies) (cm^{-3})	1.0×10^{12}	1.0×10^{12}	1.0×10^{12}

3. RESULTS AND DISCUSSION

Validation of simulated device with experimental work

First, a simulation of a similar device with ITO/ TiC_3T_x/$MAPbI_3$/Ag architecture reported by Du et al., (2022b) experimentally was done. The experimental data was extracted using the digitizer tool in Origin 2018 software. Table 4 shows the comparison of the experimental and simulated solar cell parameters.

Table 3 Comparison of the output parameters of the simulated and experimental device

ITO/$Ti_3C_2T_x$/$MAPbI_3$/PCBM/Ag Device	**V_{OC} (V)**	**J_{SC} (mA/cm^2)**	**FF (%)**	**PCE (%)**
Simulated	0.9118	20.88	69.20	13.18
Experimental	0.9800	19.10	59.43	11.12

The feasibility and validity of our simulation's material parameters and device configuration are demonstrated by the reasonably good agreement between the simulated and experimental results.

Device optimization

The optimization of the photovoltaic performance of the device with MXene as HTL was done by varying the ETL, HTL and absorber doping concentrations, absorber defect density, MXene layer thickness and the defect density at the interfaces.

The effect of ETL doping concentration, N_D on the device's photovoltaic performance

It has been reported that adding an n-type dopant in PCBM improves its conductivity and hence accelerates the extraction of electrons. This tends to reduce the accumulation of carriers at the interface, which in turn suppresses charge recombination (Wang et al., 2023). In this simulation, the ETL doping concentration, N_D was varied from 10^{10} – 10^{20} cm^{-3}, as depicted in Figure 2.

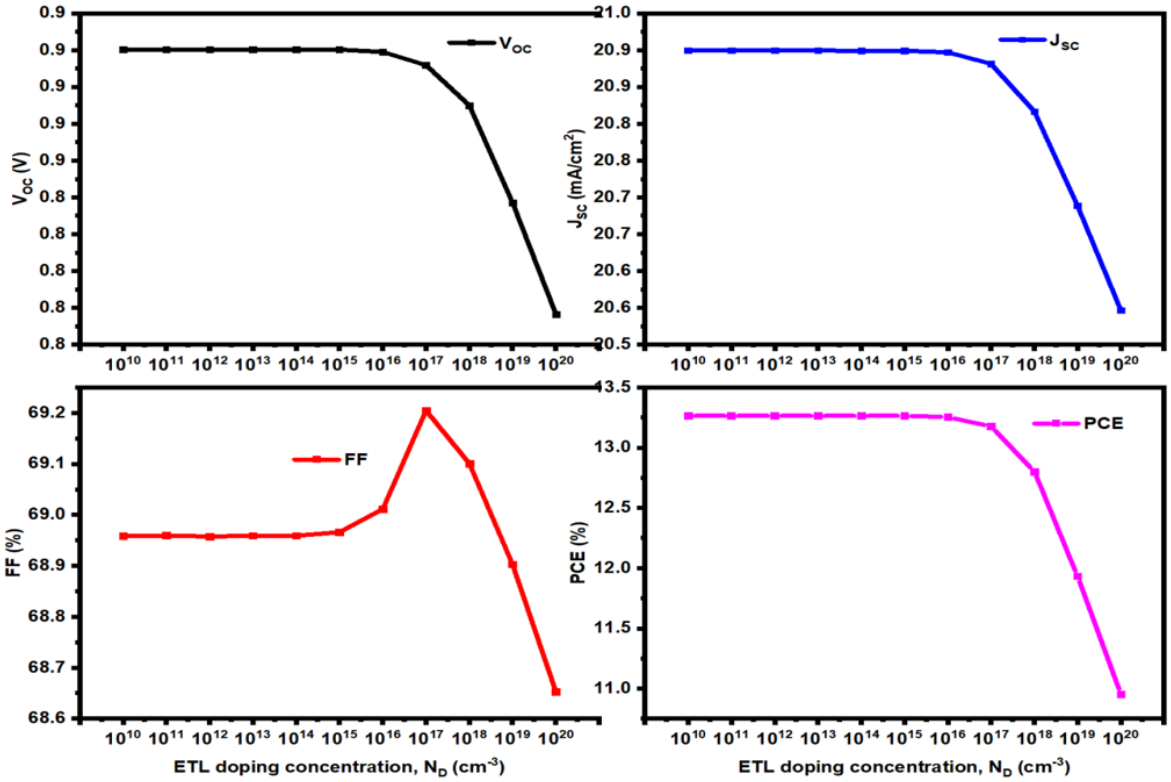

Figure 2 Variation of PSC metrics with ETL doping concentration, N_D

The V_{OC} remained constant as N_D increased from $10^{10} – 10^{15}$ cm^{-3}, then dropped drastically to 0.7765 V at 10^{20} cm^{-3}. Similarly, J_{SC} value remained constant as N_D increased from $10^{10} – 10^{15}$ cm^{-3} before dropping drastically to 20.55 mA/ cm^{-2} at 10^{20} cm^{-3}. On the other hand, the FF increased from 68.96 – 69.20 % when N_D was varied from $10^{10} – 10^{17}$ cm^{-3} then dropped to 68.65 % as N_D was further increased to 10^{20} cm^{-3}. The device's PCE was observed to remain constant as N_D increased from $10^{10} – 10^{15}$, before dropping to 10.95 % at 10^{20} cm^{-3}. The reduction of V_{OC}, J_{SC}, PCE when N_D exceeded 10^{15} and FF when ND exceeded 10^{16}, emanates from the fact that too high ETL doping concentration shortens radiative lifetimes lowering carrier mobilities hence carrier diffusion length (Sinha et al., 2023). The optimal photovoltaic parameters were obtained for an ETL doping concentration of 10^{15}; V_{OC} = 0.9202 V, J_{SC} = 20.90 mA/cm^{-2}, FF = 68.97 % and PCE = 13.26 %.

The effect of HTL doping concentration, N_A on the device's photovoltaic performance

In perovskite solar cells, the HTLs are significant in ensuring efficient transfer of holes at the HTL/perovskite interface and also enhancing the film crystallization. Therefore, it is imperative to determine an ideal HTL material with a suitable acceptor doping concentration, N_A for improved PSC performance. TiC_3T_x Mxene has been reported to possess excellent properties like high hole mobility and superior metallic conductivity suitable to enhance hole extraction across the Mxene/perovskite interface which improves the device's PCE (Palei et al., 2023).

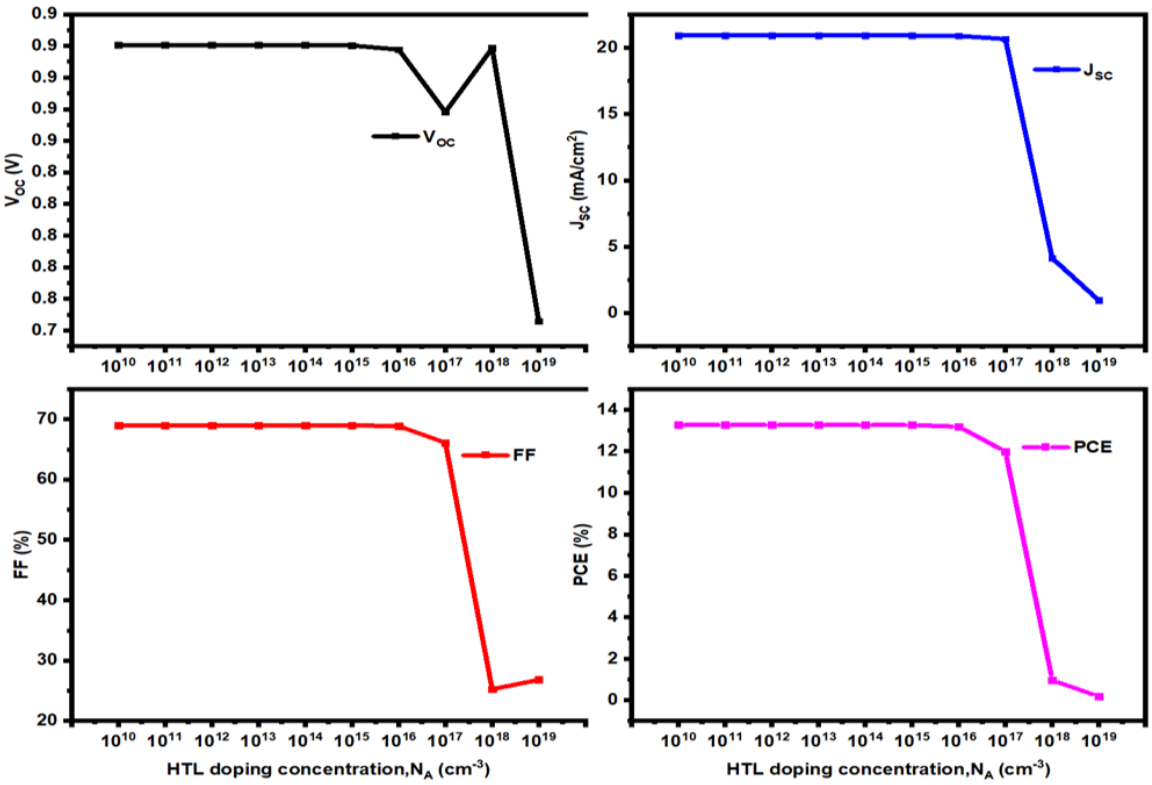

Figure 3 Variation of the PSC metrics with Mxene doping concentration, N_A

In this simulation, the Mxene doping concentration, N_A was varied in the range of $10^{10} – 10^{19}$ cm^{-3}, as shown in Figure 3. The V_{OC}, remained constant as N_A increased from $10^{10} – 10^{14}$ cm^{-3}, after which it declined up to $N_A = 10^{17}$ cm^{-3}, increased slightly at 10^{18} cm^{-3} before dropping again at 10^{19} cm^{-3}. However, J_{SC}, FF and PCE remained constant as N_A was raised from 10^{10} -10^{14} cm^{-3}, after which they declined at higher values. The optimal parameters obtained at $N_A = 10^{14}$ cm^{-3} were V_{OC} = 0.9205 V, J_{SC} = 20.90 mA/cm^2, FF = 68.97 % and PCE = 13.27 %.

The influence of doping concentration in the absorber material

The acceptor doping concentration, N_A was varied in the range of $10^{10} – 10^{17}cm^{-3}$. The V_{OC} increased progressively as N_A was raised from 10^{10}-10^{16} cm^{-3}, but decreased when N_A reached 10^{17} cm^{-3}. In contrast, J_{SC} remained nearly constant between from $10^{10} – 10^{15}$ cm^{-3} before declining at higher doping levels, particularly at 10^{17} cm^{-3}. The FF remained nearly constant as N_A increased from $10^{10} – 10^{14}$ cm^{-3} after which it declined with further increases up to 10^{17} cm^{-3}. PCE increased steadily as N_A was raised between 10^{10} -10^{16}, cm^{-3} but decreased at 10^{17} cm^{-3}. Reportedly, very high doping concentration inhibits the transportation of holes from the HTL to the absorber due to increased recombination rate and impurity scattering in the absorber (Danladi et al., 2023). This explains the decline in J_{SC} as N_A was raised beyond 10^{15} cm^{-3}. Additionally, it has been reported that increasing absorbers acceptor doping concentration raises the V_{OC} and FF due to a stronger built-in electric field (Danladi et al., 2023) , which explains the increase in V_{OC} with N_A. Generally, doping the absorber layer with an acceptor material improves its quality performance as was seen with the increase of the PSC parameters. The optimal metrics obtained at $N_A = 10^{16}$ cm^{-3} were a V_{OC} = 0.9205 V, J_{SC} = 20.90 mA/cm^2, FF = 68.97 % and PCE = 13.27 %.

The impact of absorber defect density, N_t on the device's metric parameters

The photovoltaic parameters of a perovskite solar cell are greatly impacted by defects in the absorber layer. Most common defects include vacancies, antisites, interstials, surface defects and grain boundaries due to their low formation energy (Ye et al., 2021). When the film quality is poor, the absorber develops a high density of defects that serve as trap sites for photogenerated carriers, thereby increasing non-radiative recombination and reducing both the V_{OC} and PCE of the device (Li et al., 2020).

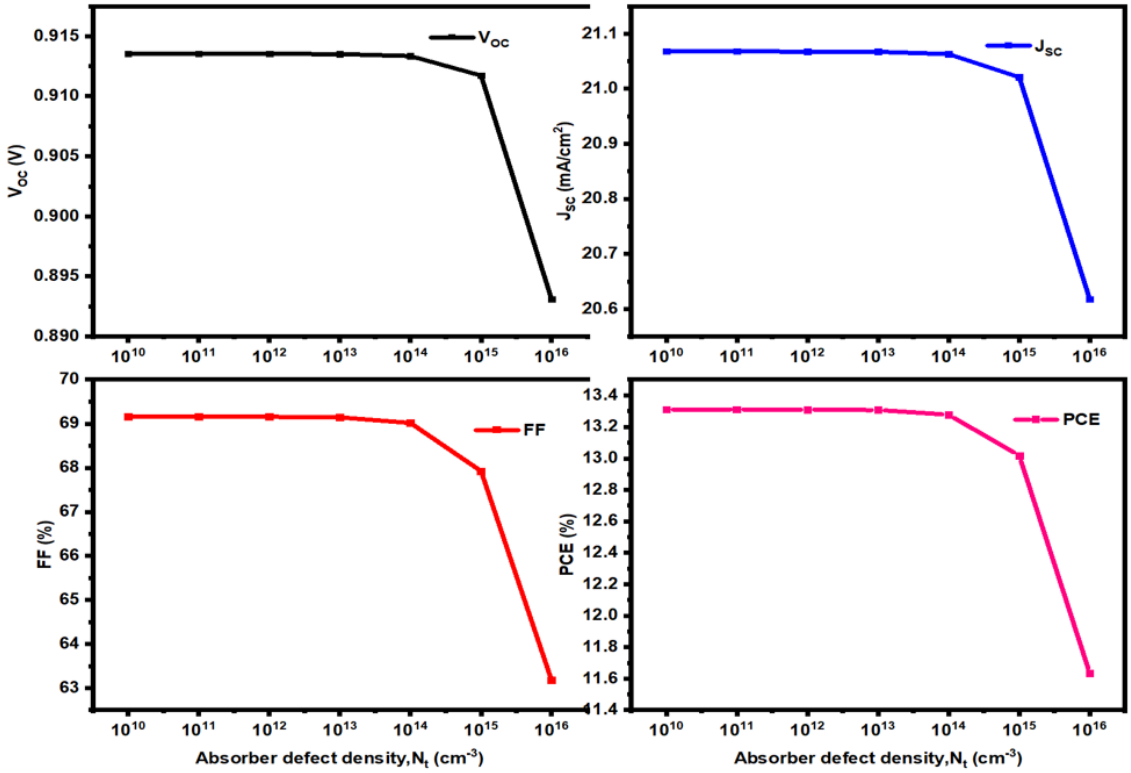

Figure 4 Variation of the device's V_{OC}, J_{SC}, FF and PCE with the absorber defect density, N_t

In this work, the effect of the absorber defect density was examined in details based on the Shockely-Read-Hall (SRH) recombination model (Goudon et al., 2007). Figure 4 depicts the variation of the solar cell parameters with absorber defect density. The absorber defect density was varied in the range of 10^{10} - 10^{16} cm^{-3}. The V_{OC}, J_{SC}, FF and PCE of the device were oberved to detororiate when the absober defect density exceeded 10^{14} cm^{-3}. $N_t = 10^{10}$ cm^{-3} was selected a s the optimal value giving V_{OC} = 0.9135 V, J_{SC} = 21. 07 mA/cm^2, FF = 69.16 % and PCE = 13.31 %.

Impact of interface defect density, N_t (HTL-absorber)

Interface defects serve as recombination centers for photogenerated carriers, reducing their collection efficiency and consequently degrading the overall device performance (George et al., 2025). The interface defect density was varied in the range of 10^{05} – 10^{16} cm^{-3}, displayed in Figure 5.

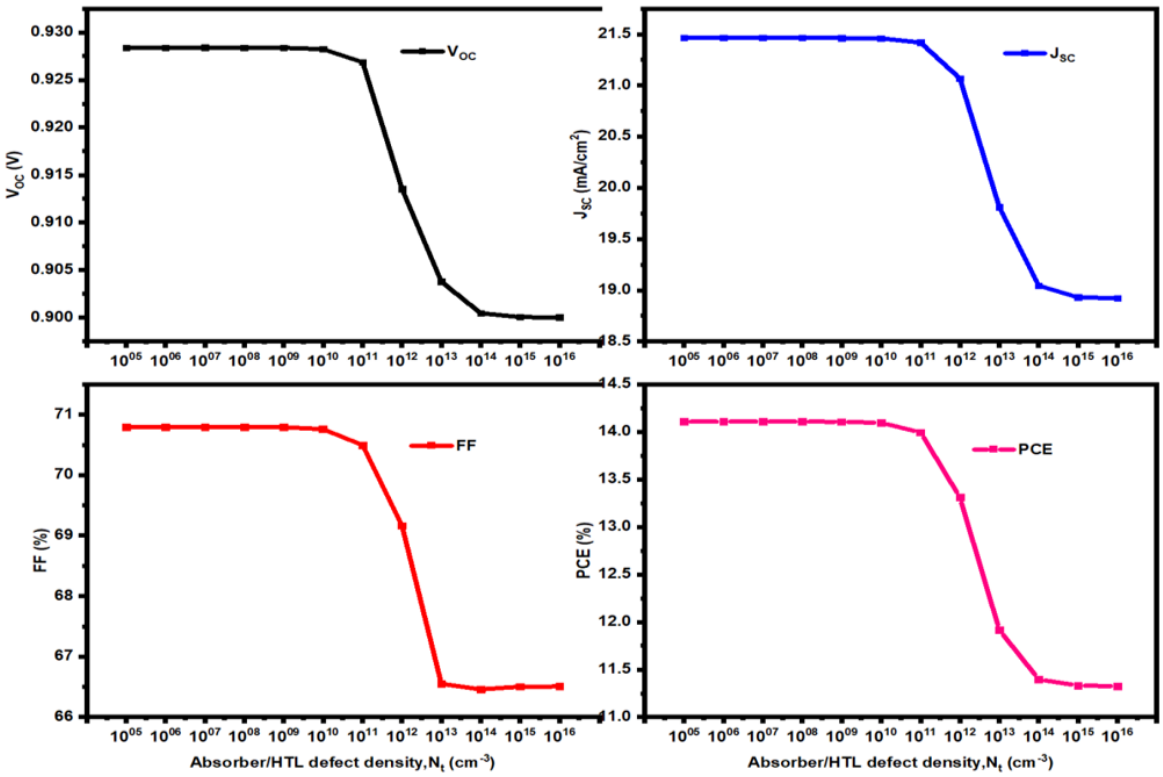

Figure 5 Variation of VOC, JSC, FF and PCE with absorber-HTL defect density, Nt

All the metric parameters remained nearly constant as Nt was raised from 10^{05} to 10^{11} cm^{-3} beyond which they declined. The optimal metric parameters obtained were; V_{OC} = 0.9284 V, J_{SC} = 21.46 mA/cm^2, FF = 70.79 %, PCE = 14.11 % for Nt = 10^{05} cm^{-3}.

Impact of interface defect density, N_t (ETL-absorber)

The impact of the defect density at the ETL-absorber interface was examined by varying the defect density from 10^{12} -10^{16} cm^{-3}. The V_{OC}, J_{SC}, FF, and PCE were seen to deteriorate when N_t exceeded 10^{14} cm^{-3}. The optimal N_t value was selected to be 10^{12} cm^{-3} which gave V_{OC} =0.9284 V, J_{SC} = 21.46 mA/cm^2, FF = 70.79 % and PCE = 14.11 %.

The influence of Mxene layer thickness on the metric parameters of the solar cell

MXene thickness was increased from 10 – 50 nm in steps of 5 nm. The variation of V_{OC}, J_{SC}, FF and PCE with Mxene thickness is depicted in Figure 6. It was noted that as Mxene thickness increased, the V_{OC} increased slightly from 0.9271 – 0.9294 V. This shows that the HTL thickness did not have a significant influence on the open circuit voltage. Conversely, the J_{SC} decreased from 21.59 to 21.32 mA/ cm^2 as the MXene thickness increased from 10 to 50 nm. This reduction can be attributed to the increased series and shunt resistances associated with the thicker HTL, which impede charge transport, enhance carrier recombination losses, and hinder efficient hole extraction from the perovskite absorber to the anode (Bouziane et al., 2025). The FF increased from 70. 38 -71.16 % as MXene thickness increased. However, the PCE of the device was observed to rise as MXene thickness was increased from 10 -35 nm, then it began to drop as the MXene thickness was further increased to 50 nm. The optimal thickness for the MXene layer, was selected to be 35 nm giving V_{OC} = 0.9287 V, J_{SC}= 21.43 mA/cm^2, FF = 70.90 % and PCE = 14.11 %.

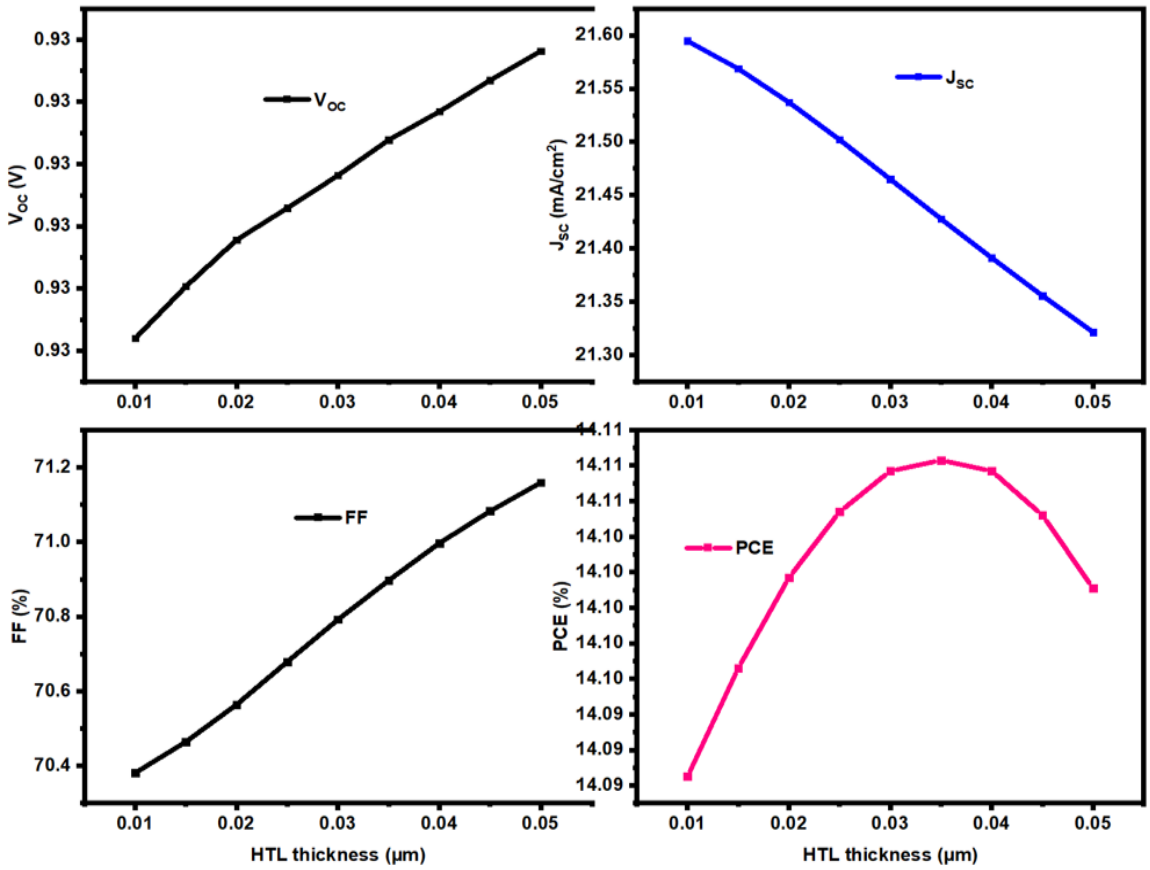

Figure 6 Variation of PSC V_{OC}, J_{SC}, FF and PCE with MXene layer thickness

Photovoltaic performance of optimized device

The optimal PSC parameters layers' doping concentrations, absorber defect density, HTL thickness and interface defects are displayed in Table 5.

Table 4 Device optimized parameters

Optimized parameters	**ETL**	**HTL**	**Absorber**	**HTL-absorber**	**ETL-Absorber**
N_A (cm^{-3})	–	10^{14}	10^{16}	10^{05}	–
N_D (cm^{-3})	10^{15}	–	-	–	–
N_t (cm^{-3})	–	–	10^{10}	10^{05}	10^{12}
Thickness (nm)	–	35	–	–	–

Figure 7(a) &(b) depicts a comparison of the J-V and EQE curves obtained at the start of the simulation and after optimization. The device's metrics were significantly enhanced after optimizing the ETL, HTL & absorber doping concentrations, absorber defect density, interface defect density and the HTL layer thickness as shown in in Table 6. The EQE curve was used to show the effectiveness of the device photon conversion in the spectral range of 300 – 900 nm. At the start of the simulation, the EQE increased to 64.36 % at 300 nm, reached a maximum of 94.09 % at 370 nm and then decreased to 0 % at 900 nm. After optimization, the EQE obtained at 300 nm was 71.03 %, then it increased to 98.26 % at 370 nm before dropping to 0 % at 900 nm. This shows that optimizing the device parameters improves the conversion of photon energy, enhancing the device's performance.

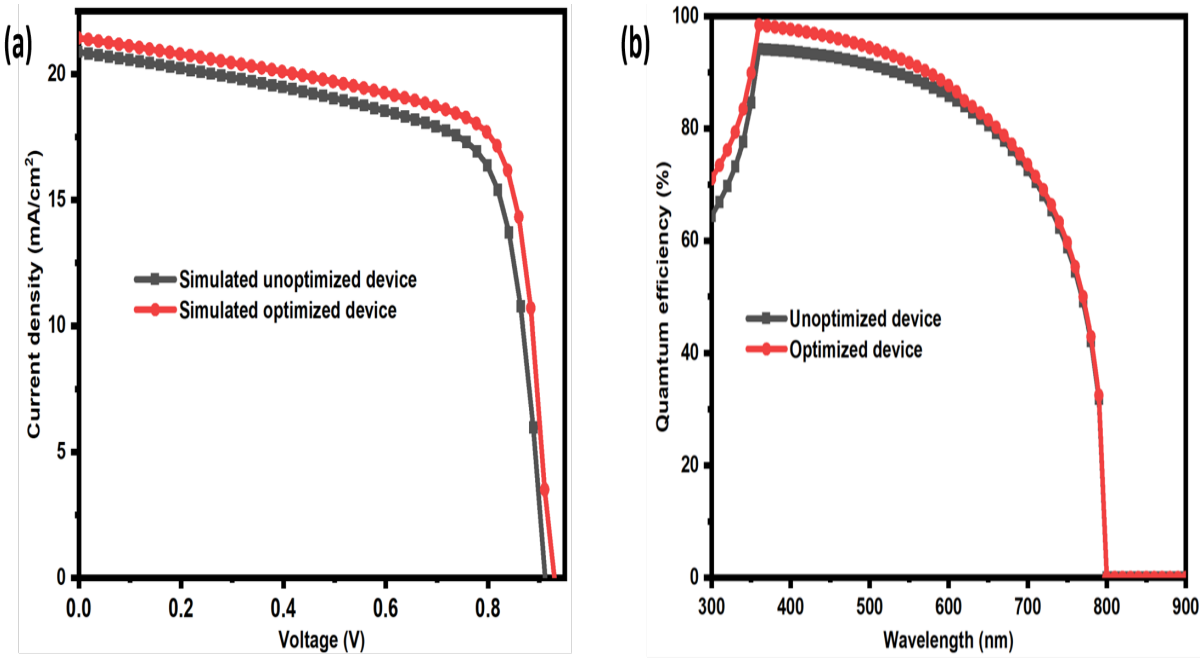

Figure 7 Comparison of (a) J-V curves and (b) EQE curves obtained at the start of the simulation and after optimization

A comparison of the simulated results at the start and after optimization process is shown in Table 6.

Table 5 Comparison of simulated results at the start and after optimization

ITO/$Ti_3C_2T_x$/$MAPbI_3$/PCBM/Ag Device	**V_{OC} (V)**	**J_{SC} (mA/cm²)**	**FF (%)**	**PCE (%)**
Simulated (start)	0.9118	20.88	69.20	13.18
Simulated (optimized)	0.9287	21.43	70.90	14.11

4. CONCLUSION

In this study, a perovskite solar cell employing $Ti_3C_2T_x$ MXene as the hole transport layer (HTL) with the configuration ITO/$Ti_3C_2T_x$/$MAPbI_3$/PCBM/Ag was simulated using SCAPS-1D software. The experimental performance of a comparable device has been reported in the literature, and our initial simulation results show good agreement with these findings, thereby validating the feasibility of the chosen simulation parameters. With the initial simulation parameters, the device gave a PCE = 13.18 %, V_{OC} = 0.9118 V, J_{SC} = 20.88 mA/cm² and FF = 69.20 %. The influence of absorber defect density, ETL, HTL & absorber doping concentrations, MXene thickness, and interface defect densities was also simulated and the results analysed in details. After optimization, the final simulation showed an improvement in the device metrics, giving a PCE = 14.11 %, V_{OC} = 0.9287 V, J_{SC} = 21.43 mA/cm² and FF= 70.90 %. The simulated results suggest that optimizing the device parameters like doping concentrations, defect densities and MXene thickness could help enhance the performance of the PSC experimentally.

5. ACKNOWLEDGEMENT

The authors gratefully acknowledge Professor Marc Burgelman and his team at the Department of Electronics and Information Systems, University of Ghent, Belgium, for developing the SCAPS-1D software package and for granting permission to use it.

REFERENCES

Babar, Z.B., Sodagar, E., Rizwan, K., Sikandar, G., 2023. Introduction to MXenes, in: Rizwan, K., Khan, A., Ahmed Asiri, A.M. (Eds.), Handbook of Functionalized Nanostructured MXenes: Synthetic Strategies and Applications from Energy to Environment Sustainability. Springer Nature, Singapore, pp. 1–13. https://doi.org/10.1007/978-981-99-2038-9_1

Baraneedharan, P., Sekar, S., Murugesan, S., Ahamada, D., Mohamed, S.A.B., Lee, Y., Lee, S., 2024. Recent Advances and Remaining Challenges in Perovskite Solar Cell Components for Innovative Photovoltaics. Nanomaterials 14, 1867. https://doi.org/10.3390/nano14231867

Bhattarai, S., Borah, D., Rout, J., Pandey, R., Madan, J., Hossain, I., Handique, P., Ansari, M.Z., Hossain, M.K., Rahman, M.F., 2023. Designing an efficient lead-free perovskite solar cell with green-synthesized CuCrO2 and CeO2 as carrier transport materials. RSC Adv. 13, 34693–34702. https://doi.org/10.1039/D3RA06722J

Bouderbala, I.Y., Hamdi, N.E., 2023. Effects of absorber layer thickness and doping density on the performance of perovskite solar cells: a simulation analysis using SCAPS-1D software. Algerian J. Eng. Technol. 8, 131–137.

Bouziane, A., El Ghazi, H., En-nadir, R., Belaid, W., Abboudi, H., Sali, A., 2025. Effects of Doping, Transport Layer Thickness, and Composition on the Performance of Mixed Halide Perovskite Single-Junction Solar Cells. J. Electron. Mater. 54, 7296–7307. https://doi.org/10.1007/s11664-025-12093-1

Burgelman, M., Nollet, P., Degrave, S., 2000. Modelling polycrystalline semiconductor solar cells. Thin Solid Films 361–362, 527–532. https://doi.org/10.1016/S0040-6090(99)00825-1

Danladi, E., Egbugha, A.C., Obasi, R.C., Tasie, N.N., Achem, C.U., Haruna, I.S., Ezeh, L.O., 2023. Defect and doping concentration study with series and shunt resistance influence on graphene modified perovskite solar cell: A numerical investigation in SCAPS-1D framework. J. Indian Chem. Soc. 100, 101001. https://doi.org/10.1016/j.jics.2023.101001

Dar, S.A., Sengar, B.S., 2024. Optimization and Performance Analysis of Inorganic Lead-Free CsSnBr3 Perovskite Solar Cells Using Diverse Electron Transport Materials. Energy Fuels 38, 8229–8248. https://doi.org/10.1021/acs.energyfuels.4c00953

Diouf, B., Muley, A., Pode, R., 2023. Issues, Challenges, and Future Perspectives of Perovskites for Energy Conversion Applications. Energies 16, 6498. https://doi.org/10.3390/en16186498

Du, J.-B., Yang, L., Jin, X., Liu, C.-L., Wang, H.-H., Wang, X.-F., 2022a. Spray deposition of vinyl tris(2-methoxyethoxy) silane-doped Ti3C2Tx MXene hole transporting layer for planar perovskite solar cells. J. Alloys Compd. 900, 163372. https://doi.org/10.1016/j.jallcom.2021.163372

Du, J.-B., Yang, L., Jin, X., Liu, C.-L., Wang, H.-H., Wang, X.-F., 2022b. Spray deposition of vinyl tris(2-methoxyethoxy) silane-doped Ti3C2Tx MXene hole transporting layer for planar perovskite solar cells. J. Alloys Compd. 900, 163372. https://doi.org/10.1016/j.jallcom.2021.163372

George, V.S., Rasu Chettiar, A.-D., Rajendran, S., Bencherif, H., Sasikumar, P., Marasamy, L., 2025. Modelling Insights of Sb2(S,Se)3 Solar Cells Using Triazatruxene Hole Transport Layers. Adv. Theory Simul. https://doi.org/10.1002/adts.202500487

Goudon, T., Miljanovic, V., Schmeiser, C., 2007. On the Shockley-Read-Hall Model: Generation-Recombination in Semiconductors. SIAM J. Appl. Math. 67, 1183–1201. https://doi.org/10.1137/060650751

Guo, Z., Gao, L., Xu, Z., Teo, S., Zhang, C., Kamata, Y., Hayase, S., Ma, T., 2018. High Electrical Conductivity 2D MXene Serves as Additive of Perovskite for Efficient Solar Cells. Small Weinh. Bergstr. Ger. 14, e1802738. https://doi.org/10.1002/smll.201802738

He, J., Armstrong, J., Cong, P., Menagen, B., Igaher, L., Beale, A.M., Etgar, L., Avnir, D., 2020. Affecting an Ultra-High Work Function of Silver. Angew. Chem. Int. Ed. 59, 4698–4704. https://doi.org/10.1002/anie.201912293

Hossain, M.K., Toki, G.F.I., Samajdar, D.P., Mushtaq, M., Rubel, M.H.K., Pandey, R., Madan, J., Mohammed, M.K.A., Islam, Md.R., Rahman, Md.F., Bencherif, H., 2023. Deep Insights into the Coupled Optoelectronic and Photovoltaic Analysis of Lead-Free CsSnI3 Perovskite-Based Solar Cell Using DFT Calculations and SCAPS-1D Simulations. ACS Omega 8, 22466–22485. https://doi.org/10.1021/acsomega.3c00306

Hoy, N.W., Noto, L.L., Mbule, P.S., 2025. SCAPS-1D simulation of perovskite solar cells with hydroxyapatite scaffold for lead encapsulation and performance optimization. Mater. 9, 101260. https://doi.org/10.1016/j.nxmate.2025.101260

Husainat, A., Ali, W., Cofie, P., Attia, J., Fuller, J., 2019. Simulation and analysis of methylammonium lead iodide (CH3NH3PbI3) perovskite solar cell with Au contact using SCAPS 1D simulator. Am. J. Opt. Photonics 7, 33.

Jayan K, D., Sebastian, V., 2021. Comprehensive device modelling and performance analysis of MASnI3 based perovskite solar cells with diverse ETM, HTM and back metal contacts. Sol. Energy 217, 40–48. https://doi.org/10.1016/j.solener.2021.01.058

Karmaker, H., Siddique, A., Das, B.K., Islam, M.N., 2024. Modeling and performance investigation of novel inorganic Cs4CuSb2Cl12 nanocrystal perovskite solar cell using SCAPS-1D. Results Eng. 22, 102106. https://doi.org/10.1016/j.rineng.2024.102106

Li, B., Chang, B., Pan, L., Zihao, L., Fu, L., He, Z., Yin, L., 2020. Tin-Based Defects and Passivation Strategies in Tin-Related Perovskite Solar Cells. ACS Energy Lett. 5, 3752–3772. https://doi.org/10.1021/acsenergylett.0c01796

Liu, S., Biju, V.P., Qi, Y., Chen, W., Liu, Z., 2023. Recent progress in the development of high-efficiency inverted perovskite solar cells. NPG Asia Mater. 15, 1–28. https://doi.org/10.1038/s41427-023-00474-z

Nahid, M.N., Shah, M.S., Mamur, H., Hosen, R., Bhuiyan, M.R.A., 2024. Optimizing lead-free CH3NH3SnI3 perovskite solar cells by using SCAPS-1D software. Chem. Inorg. Mater. 4, 100069. https://doi.org/10.1016/j.cinorg.2024.100069

Palei, S., Murali, G., Kim, C.-H., In, I., Lee, S.-Y., Park, S.-J., 2023. A Review on Interface Engineering of MXenes for Perovskite Solar Cells. Nano-Micro Lett. 15, 123. https://doi.org/10.1007/s40820-023-01083-9

Qamar, S., Fatima, K., Ullah, N., Akhter, Z., Waseem, A., Sultan, M., 2022. Recent progress in use of MXene in perovskite solar cells: for interfacial modification, work-function tuning and additive engineering. Nanoscale 14, 13018–13039. https://doi.org/10.1039/D2NR02799B

Salim, O., Mahmoud, K.A., Pant, K.K., Joshi, R.K., 2019. Introduction to MXenes: synthesis and characteristics. Mater. Today Chem. 14, 100191. https://doi.org/10.1016/j.mtchem.2019.08.010

Sharma, S., Kumar, K., Pachuari, R.K., Kuchhal, P., Vardhan, A.S.S., Khan, B., Ali, A., 2024. Numerical simulations, design and modeling of methylammonium tin iodide halide-based single-junction perovskite solar cell. Electr. Eng. 106, 1225–1239. https://doi.org/10.1007/s00202-023-02166-x

Sinha, N.K., Roy, P., Ghosh, D.S., Khare, A., 2023. Investigation of effect of doping in perovskite solar cells: A numerical simulation approach. Mater. Today Proc., Recent Advances in Material Science and Organic Synthesis 83, 6–13. https://doi.org/10.1016/j.matpr.2022.10.006

Teli, A.M., Mane, S.M., Mishra, R.K., Jeon, W., Shin, J.C., 2025. Unlocking the Potential of Ti3C2Tx MXene: Present Trends and Future Developments of Gas Sensing. Micromachines 16, 159. https://doi.org/10.3390/mi16020159

Uddin, Md.S., Hosen, R., Sikder, S., Mamur, H., Bhuiyan, M.R.A., 2024. Photovoltaic performance enhancement of Al/ZnO:Al/i-ZnO/CdS /CIGS/Pt solar cell using SCAPS-1D software. Energy 2, 100080. https://doi.org/10.1016/j.nxener.2023.100080

Wang, J., Cai, Z., Lin, D., Chen, K., Zhao, L., Xie, F., Su, R., Xie, W., Liu, P., Zhu, R., 2021. Plasma Oxidized Ti3C2Tx MXene as Electron Transport Layer for Efficient Perovskite Solar Cells. ACS Appl. Mater. Interfaces 13, 32495–32502. https://doi.org/10.1021/acsami.1c07146

Wang, S., Chen, Z., Zhao, G., Wang, F., 2023. Quantum confinement effect on the electronic and optical properties of two-dimensional halide perovskites. Comput. Mater. Sci. 230, 112524. https://doi.org/10.1016/j.commatsci.2023.112524

Wang, Y., Xia, Z., Liu, Y., Zhou, H., 2015. Simulation of perovskite solar cells with inorganic hole transporting materials, in: 2015 IEEE 42nd Photovoltaic Specialist Conference (PVSC). Presented at the 2015 IEEE 42nd Photovoltaic Specialist Conference (PVSC), pp. 1–4. https://doi.org/10.1109/PVSC.2015.7355717

Yan, K., Sun, B., Lu, T., Feng, X.-D., 2023. Simulation of MASnI3-based inverted perovskite solar cells with double hole transport layers and an electron transport layer. Optik 287, 171100. https://doi.org/10.1016/j.ijleo.2023.171100

Yang, C., Hu, W., Liu, J., Han, C., Gao, Q., Mei, A., Zhou, Y., Guo, F., Han, H., 2024. Achievements, challenges, and future prospects for industrialization of perovskite solar cells. Light Sci. Appl. 13, 227. https://doi.org/10.1038/s41377-024-01461-x

Yang, L., Li, P., Ma, J., Zhang, X., Wang, X.-F., Liu, Y., 2023. MXenes for perovskite solar cells: Progress and prospects. J. Energy Chem. 81, 443–461. https://doi.org/10.1016/j.jechem.2023.02.041

Ye, J., Byranvand, M.M., Martínez, C.O., Hoye, R.L.Z., Saliba, M., Polavarapu, L., 2021. Defect Passivation in Lead-Halide Perovskite Nanocrystals and Thin Films: Toward Efficient LEDs and Solar Cells. Angew. Chem. Int. Ed Engl. 60, 21636–21660. https://doi.org/10.1002/anie.202102360